

Cooling Injection Effect on a Transonic Squealer Tip—Part I: Experimental Heat Transfer Results and CFD Validation

H. Ma

University of Michigan-Shanghai
Jiao Tong University Joint Institute,
Shanghai 200240, China
e-mail: haitengma@gmail.com

Q. Zhang¹

Department of Mechanical Engineering
and Aeronautics,
School of Engineering
and Mathematical Sciences,
City, University of London,
Northampton Square,
London EC1V 0HB, UK
e-mail: Qiang.Zhang.1@city.ac.uk

L. He

Department of Engineering Science,
University of Oxford,
Oxford OX2 0ES, UK
e-mail: Li.He@eng.ox.ac.uk

Z. Wang

University of Michigan-Shanghai
Jiao Tong University Joint Institute,
Shanghai 200240, China
e-mail: wangzhaoguang1991@hotmail.com

L. Wang

University of Michigan-Shanghai
Jiao Tong University Joint Institute,
Shanghai 200240, China
e-mail: lipo.wang@sjtu.edu.cn

Recent studies have demonstrated that the aerothermal characteristics of turbine rotor blade tip under a transonic condition are qualitatively different from those under a low-speed subsonic condition. The cooling injection adds further complexity to the over-tip-leakage (OTL) transonic flow behavior and aerothermal performance, particularly for commonly studied shrouded tip configurations such as a squealer tip. However there has been no published experimental study of a cooled transonic squealer. The present study investigates the effect of cooling injection on a transonic squealer through a closely combined experimental and CFD effort. Part I of this two-part paper presents the first of the kind tip cooling experimental data obtained in a transonic linear cascade environment (exit Mach number 0.95). Transient thermal measurements are carried out for an uncooled squealer tip and six cooling configurations with different locations and numbers of discrete holes. High-resolution distributions of heat transfer coefficient and cooling effectiveness are obtained. ANSYS FLUENT is employed to perform numerical simulations for all the experimental cases. The mesh and turbulence modeling dependence is first evaluated before further computational studies are carried out. Both the experimental and computational results consistently illustrate strong interactions between the OTL flow and cooling injection. When the cooling injection (even with a relatively small amount) is introduced, distinctive series of stripes in surface heat transfer coefficient are observed with an opposite trend in the chordwise variations on the squealer cavity floor and on the suction surface rim. Both experimental and CFD results have also consistently shown interesting signatures of the strong OTL flow-cooling interactions in terms of the net heat flux reduction distribution in areas seemingly unreachable by the coolant. Further examinations and analyses of the related flow physics and underlining vortical flow structures will be presented in Part II. [DOI: 10.1115/1.4035175]

1 Introduction

The rotor blade tip is the most vulnerable part in high-pressure (HP) turbine. In addition to being a major contributor to the loss of turbine efficiency, the over-tip-leakage (OTL) flow introduces very high thermal load to the tip and casing. The tip cooling design has always been a challenging task due to the complex OTL flow behavior and its interaction with cooling injection.

Researches on the blade tip heat transfer have been carried out extensively in the past three decades. A thorough review was provided by Bunker [1] about 15 years ago. More understanding has been gained through the recent research efforts gradually moving from simplified low-speed condition to more engine-realistic high-speed environment.

The early work by Mayle and Metzger [2] measured the averaged heat transfer coefficient on a modeled flat tip in a low-speed condition. They also established the wisdom of pressure-driven mechanism for the tip gap flow. Bunker et al. [3] reported “central sweet spot” of low heat transfer within the thickest portion of the tip in their experiments ($M_{\text{exit}} = 0.75$). A complementary study by Ameri and Bunker [4] showed good comparison between the experimental data and the numerical results using a radius edge tip model. In a low-speed condition, Newton et al. [5] and Krishnababu et al. [6] showed that the maximum heat transfer coefficient occurs on the flow reattachment region near the pressure side rim.

The aerothermal behavior of the squealer tip has been widely studied, mostly under subsonic conditions. The effect of cavity depth was presented by Metzger et al. [7], Chyu et al. [8], and Bunker and Bailey [9]. They all found that increasing the cavity depth reduces the heat transfer on the cavity floor. The effects of tip gap height, squealer geometry arrangement on blade tip heat transfer were presented by Azad et al. [10,11] and Kwak et al. [12]. Their results showed that increasing the tip clearance would bring up the heat transfer level and the suction side squealer outperforms the full squealer in terms of decreasing the overall tip heat transfer. Another parametric study by Zhou and Hodson [13] found that thinner squealer rim could lower the average heat transfer coefficient on the tip.

The primary goal of the tip cooling is to reduce the heat load and help the tip survive the extremely hot gas temperature, as addressed by Bunker [14]. For a subsonic flat blade tip ($M_{\text{exit}} = 0.6$), Kwak and Han [15] found that higher blowing ratios would decrease the heat transfer coefficient and increase the film cooling effectiveness. The effect of tip gap height on the adiabatic effectiveness and heat transfer coefficient was evaluated by Christophel et al. [16,17]. Better cooling performance is achieved for smaller tip gap due to its larger adiabatic effectiveness value. The effect of cooling hole location was evaluated by Newton et al. [18], who reported that injecting coolant inside the separation bubble would bring higher net heat flux reduction compared with injecting at the reattachment region.

The squealer tip has to be effectively cooled, especially near the thin rim region. Kwak and Han [19] and Ahn et al. [20] reported that coolant injection from both tip and pressure side holes provides higher film cooling effectiveness compared to the injection from tip holes only. The parametric study by Mhetras

¹Corresponding author.

Contributed by the Structures and Dynamics Committee of ASME for publication in the JOURNAL OF ENGINEERING FOR GAS TURBINES AND POWER. Manuscript received July 14, 2016; final manuscript received October 8, 2016; published online January 10, 2017. Editor: David Wisler.

et al. [21] found that deeper cavity brings higher effectiveness on a cutback squealer tip. Naik et al. [22] observed that the cooling effectiveness is high at the trailing edge cut of the partial squealer tip due to the exit of the tip leakage flow accumulated with coolant.

Most previous tip studies were carried out at low-speed conditions. The transonic aerothermal behavior of the over-tip-leakage (OTL) flow attracts much more attention in the recent years. Wheeler et al. [23] demonstrated the dramatic difference in tip heat transfer and flow structure between low-speed and transonic flows. For the first time, experiments by Zhang et al. [24] showed some distinct stripes of heat transfer coefficient on a transonic flat tip ($M_{\text{exit}} = 1.0$), which indicates the existence of shock waves within tip gap. Zhang et al. [25] reported that the heat transfer ranking with respect to the tip clearance is reversed in the transonic part of the blade tip compared with the subsonic part. Zhang and He [26] demonstrated the breakdown of the low-speed pressure-driven wisdom when the OTL flow is choked. They showed that, in transonic flow regime, the over tip choking caps the tip leakage mass flow rate. Similar results were later reported by Shyam et al. [27]. Zhang and He [28] also showed the strong interaction between aerodynamics and heat transfer for a transonic turbine blade tip. Other experimental studies under transonic conditions include O'Dowd et al. [29] and Anto et al. [30]. All the above studies consistently demonstrate that the conventional wisdoms at low-speed conditions need to be re-examined, while the OTL flow reaches transonic speed.

There have been a few experimental studies on the aerothermal performance of the transonic squealer tip. Dunn and Haldeman [31] measured the heat flux on a squealer tip for a rotating turbine stage at transonic conditions ($M_{\text{exit}} = 1.1$). Key and Arts [32] found that the effect of Reynolds number on the velocity of the tip gap flow is smaller than that for a flat tip ($M_{\text{exit}} = 1.1$). Viridi et al. [33] obtained the heat transfer data for a squealer tip in the high-speed linear cascade ($M_{\text{exit}} = 1.0$). The experimental data showed good agreement with the numerical results in their study.

Very little tip cooling experimental data are available in transonic condition among the open literature. O'Dowd et al. [34] experimentally investigated the aerothermal performance of a cooled winglet tip ($M_{\text{exit}} = 1.0$). There are a few numerical studies related with transonic tip cooling by Wheeler and Saleh [35], Wang et al. [36], and Zhou [37]. No experimental data have been reported so far on the squealer tip cooling under transonic conditions.

This two-part paper series aim to investigate the effect of cooling injection on a transonic squealer tip through a closely combined experimental and CFD effort. Part I presents the tip cooling experimental data obtained in a high-speed linear cascade (exit Mach number 0.95). To the authors' knowledge, this is the first set of experimental data on the squealer tip cooling under transonic conditions. The experimental data are then used to validate the capabilities of numerical solvers.

The present experimental and computational results have consistently revealed some very strong interactive phenomena between over-tip-leakage flow and cooling injection, with distinctive aerothermal signatures for a transonic squealer tip. The related aerothermal flow physics behind these phenomena will be further examined, analyzed, and discussed in the companion paper as Part II [38].

2 Experimental Setup

2.1 Experimental Facilities and Conditions. A transonic blow-down wind tunnel in the Aero-Thermal Lab, University of Michigan-Shanghai Jiao Tong University Joint Institute Shanghai, China, was employed to conduct the transient heat transfer experiment in the present study, as shown in Fig. 1. Compressed air with a maximum pressure of 3 MPa is contained in a 10 m³ air storage tank. A fisher control valve (EWT body with 667 actuator and

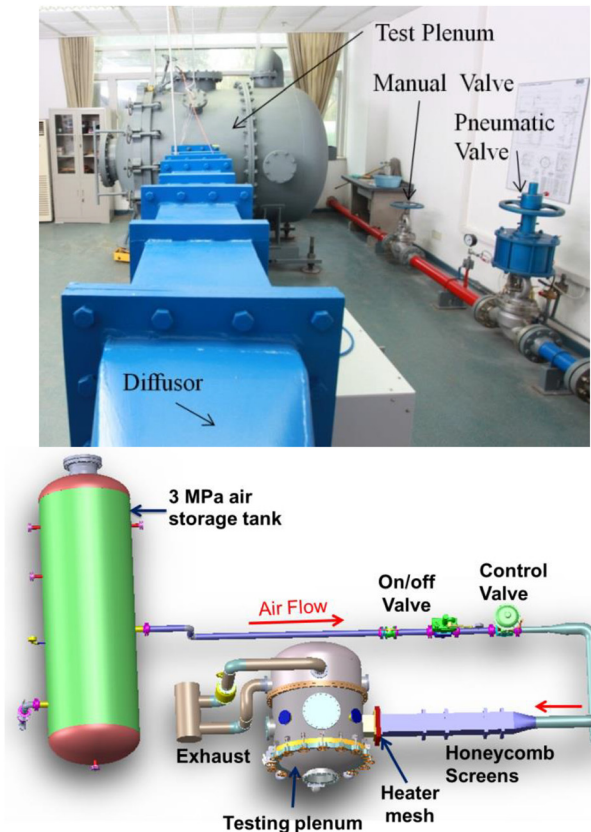


Fig. 1 Transonic wind tunnel facility in the present study

Fieldvue DVC6000 controller) regulates the total pressure at the inlet of test section in the testing plenum. An extended karman filter (EKF)-based control algorithm was developed to predicatively adjust the valve opening during the blow-down process (Zheng et al. [39], Xi et al. [40]). Honeycomb screens and flow straighteners are located downstream of the control valve to ensure the flow quality. A heater mesh (0.080 mm in width and 0.050 mm in diameter) is installed before the testing plenum to heat up the mainstream flow during the heat transfer experiment. This heater mesh is connected to a 100 kW DC power supply. The test section is located inside a testing plenum with 1.8 m in diameter. The exhaust pipeline also has a regulating valve, so the pressure of the testing plenum could be adjusted to match the Reynolds number. More details for the flow characteristic and wind tunnel design are described in Ma et al. [41], Evans et al. [42], and Chen [43].

The test section is illustrated in Fig. 2. It consists of seven blades and six passages to achieve the optimal periodicity of the flow field. There are also two boundary layer bleeds on the two sidewalls. The blade has an axial chord (C_x) of 0.039 m and is scaled from a typical high-pressure turbine blade design condition. For the three blades in the middle of the cascade, the upper part was made from resin with low thermal conductivity by stereolithography technology, and the lower part was made from steel for fixing purpose. In the present study, the tip gap height is approximately 1% of blade span.

Table 1 lists six cooled squealer tip configurations investigated in the present study. There are two cooling hole spacings: $4d$ for the nine-hole cases and $8d$ for the five-hole cases. These cooling holes are located in three different locations in tip cavity: one near the pressure side (PS), one on the camberline (CAM), and one near the suction side (SS). For all these cases, the injection angle of the cooling holes is 90 deg. The diameter of the cooling hole (d) is 1.18 times the tip gap height (g).

Secondary cooling air was produced by a vortex tube system connected to a 600 kPa compressed air supply, as shown in Fig. 2.

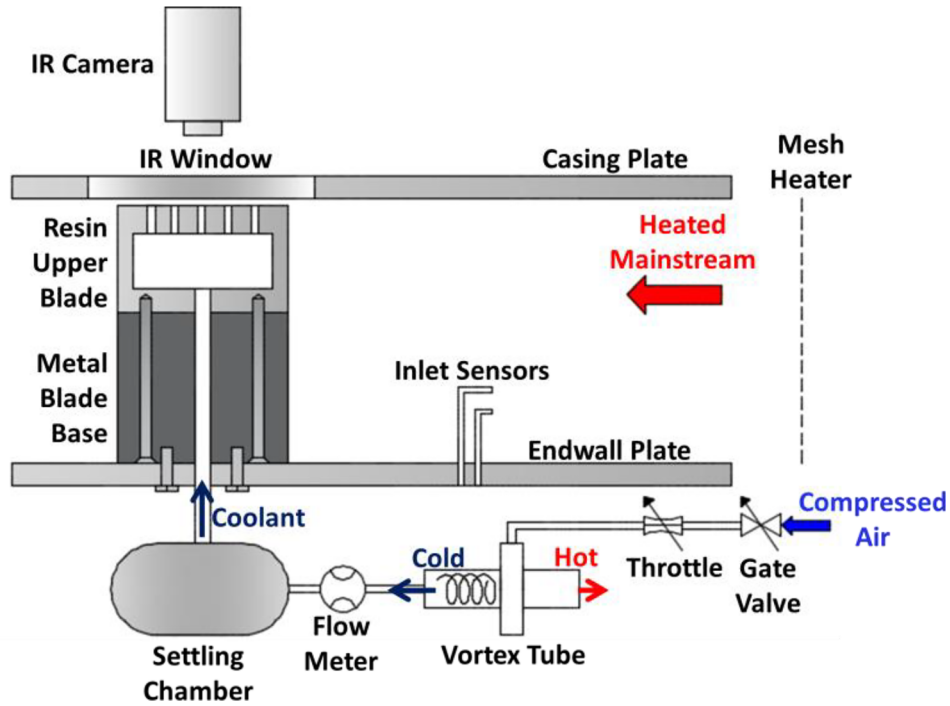
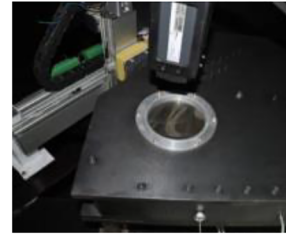
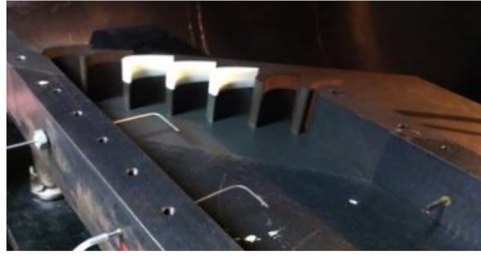
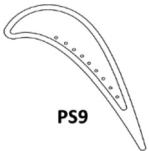
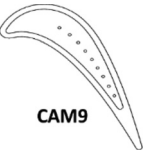

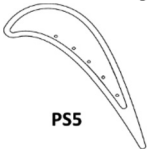
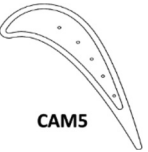



Fig. 2 Test section and the coolant supply system

Table 1 Cooled squealer tip configurations

		Location of holes		
		PS	Camber line	SS
Spacing between holes	4d			
	8d			

Before entering into the blade tip region, the cold air was stabilized in a settling chamber, where the total pressure and total temperature of the coolant were measured. The settling chamber was insulated and placed close to the test section to avoid heat addition from the environment. A near 15 K deg of temperature drop was achieved by the cooling system.

The tip surface temperature history of the central blade was recorded by a FLIR A325 Researcher infrared (IR) camera with a spatial resolution of 320×240 at a frequency of 60 Hz, through a

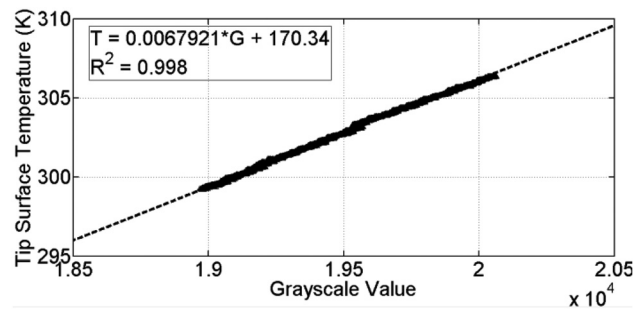


Fig. 3 IR camera calibration curve

zinc-selenide (ZnSe) IR window. To minimize the uncertainties introduced by surface emissivity, IR window transmissivity, radiation from surroundings, etc., one thermocouple was embedded in the resin tip to be flush with the tip surface in order to perform in situ calibration of the IR images during a blow-down run. The thermocouple (K-type, Omega) has a wire diameter of 0.076 mm (0.003 in.) and response time of less than 80 ms. Figure 3 shows an example of the linear calibration relation between the image grayscale values and the temperature readings from a surface thermocouple. The same type of thermocouple was employed in the inlet total temperature sensor. National instruments (NI) PXIe DAQ system was employed to acquire pressure and temperature readings.

Flow conditions for the transonic turbine blade tip heat transfer experiment are summarized in Table 2. The total pressure ratio between the coolant and the inlet mainstream is 1.1 ± 0.01 . The total temperature ratio between the coolant and the inlet mainstream is 0.9 ± 0.004 . Detailed time histories of the inlet mainstream total pressure ($P_{0,i}$) and total temperature ($T_{0,i}$), as well as the coolant total pressure ($P_{0,c}$) and total temperature ($T_{0,c}$) are illustrated in Fig. 4. The ratio between the measured coolant mass flow rate and the cascade mass flow rate in a single passage (same as engine-equivalent mass flow rate given the current height of cascade inlet) is roughly 0.45% for all the nine-hole cases and 0.26% for all the five-hole cases. The inlet turbulent intensity is approximately 1%. The coolant supply system was precooled for 30 min before the blow-down experiment to reach the thermal steady state. The heater mesh was turned on 5 s after the opening of the control valve when both the temperature and pressure of the mainstream flow were stabilized. Two seconds of the transient thermal measurement data were used for data processing. Heat penetration depth was estimated to be 1.5 mm.

2.2 Data Reduction Method. In the present study, heat transfer coefficient (HTC, h) is defined according to the Newton's law of cooling:

$$q'' = h(T_{ad} - T_w) \quad (1)$$

where q'' is the heat flux, T_w is the wall temperature, and T_{ad} is the adiabatic temperature, which is also the fluid driving temperature in heat transfer. The local recovery effect in high-speed flow will remain unchanged once the local aerodynamic field reaches its steady state. Therefore, the adiabatic temperature for the uncooled case is solely determined by the inlet mainstream total temperature (Mee et al. [44], Kays et al. [45]). For the cooled case, it is a mixture between the mainstream total temperature and the coolant temperature (Kwak and Han [19]).

During the transient thermal measurement process, the total temperatures of the inlet mainstream and the coolant both remain constant, as shown in Fig. 4. From the transient temperature history, q'' can be reconstructed using the impulse method by Oldfield [46]. This method has been employed in a series of previous studies (Zhang et al. [24,25], O'Dowd et al. [47]) and proved to be accurate, computationally efficient, and reliable. Next, for

Table 2 Flow conditions for the present experimental study

Inlet total pressure, $P_{0,i}$ (Pa)	180,000
Inlet Mach number	0.3
Inlet Reynolds number (based on C_x)	0.26×10^6
Exit static pressure, $P_{s,e}$ (Pa)	101,325
Exit Mach number	0.95
Exit Reynolds number (based on C_x)	0.88×10^6
Coolant total pressure, $P_{0,c}$ (Pa)	198,000
Cascade mass flow rate (kg/s)	3

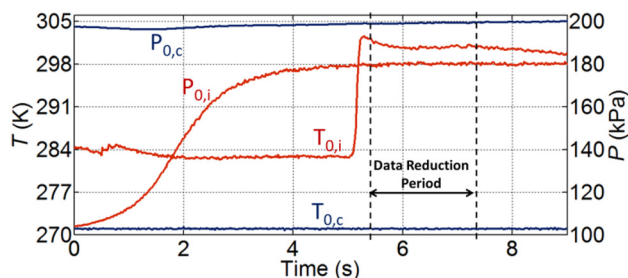


Fig. 4 Time histories of the inlet total pressure ($P_{0,i}$), total temperature ($T_{0,i}$), and coolant total pressure ($P_{0,c}$) and total temperature ($T_{0,c}$) during a blow-down run

every IR pixel location on the blade tip, h and T_{ad} can be easily obtained by the linear regression between q'' and T_w obtained during the 2 s transient time period. Figure 5 illustrates one example of the linear regression for a selected point on the tip surface. All data points are scattered evenly around the regression line. The coefficient of determination (R^2) in statistics (Devore [48]) is 0.934. The relative uncertainty in linear regression with 95% confidence (%U) is 4.9% (Coleman and Steele [49]). Such linear regression performance is highly repeatable over most of the tip surface.

To assess the reduction of the gas driving temperature by the cooling injection, cooling effectiveness is defined as (O'Dowd et al. [34])

$$\eta = \frac{T_{ad,uc} - T_{ad,c}}{T_{ad,uc} - T_{0,c}} \quad (2)$$

where $T_{ad,uc}$ is the adiabatic temperature for the uncooled case, $T_{ad,c}$ is the adiabatic temperature for the cooled case, which reflects the mixing between the coolant and mainstream temperatures, and $T_{0,c}$ is the coolant total temperature.

2.3 Uncertainty Analysis. Figure 6 shows the contours of R^2 and the relative uncertainty of heat transfer coefficient in linear regression (%U) for a cooled tip case (PS9). For most of the tip area, R^2 is above 0.92 and the relative uncertainty in linear regression is below 6%. However, near the cooling holes and the suction side rim, the linear regression performance is relatively poor, which should be caused by the lateral conduction error. Note that the overall uncertainty level reported for this cooled tip study is higher than that for the uncooled case (Ma et al [41]). This is mainly due to the increased flow unsteadiness with tip cooling injection.

Overall measurement uncertainties for the present heat transfer experiment are summarized in Table 3. With results from multiple runs, the average uncertainty values of h and η are $\pm 9.2\%$ and \pm

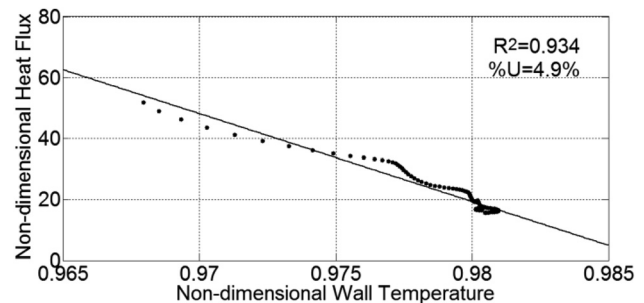


Fig. 5 Linear relationship between heat flux and wall temperature for a selected point during 2s period of transient measurement

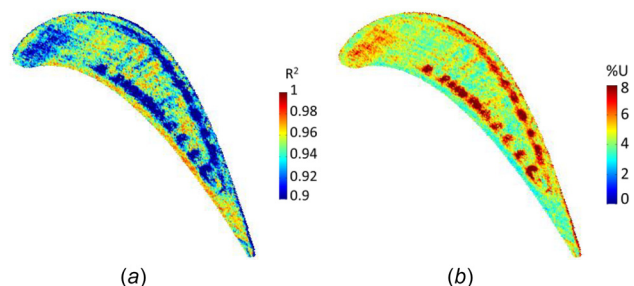


Fig. 6 Contours of (a) R^2 and (b) relative uncertainty for heat transfer coefficient in linear regression (%U) on the blade tip surface for the cooled case (PS9)

Table 3 Measurement uncertainties

Measurement	Relative uncertainty 95% confidence
Wall temperature, T_w	0.4% (300 ± 1.2 K)
Mainstream total temperature, T_0	0.4% (300 ± 1.2 K)
h	9.2%
η	12.1%

12.1%, respectively, which is within acceptable level compared to most heat transfer results in the open literature (Kwak and Han [15,19], O'Dowd et al. [34]).

3 CFD Method and Setup

ANSYS FLUENT is employed in the present study for numerical simulations. Two Reynolds-averaged Navier–Stokes (RANS) models, Spalart–Allmaras model (SA) and $k-\omega$ SST model (SST), are implemented and validated against experimental data. The computational domain is a single-blade passage with periodic boundary condition, as shown in Fig. 7. For the coolant supply system, only the feed pipes above the plenum inside the upper blade are modeled. The geometric dimensions, such as the tip gap height, the configuration of cooling holes, feed pipe length, and the blade profile, are exactly the same as the experimental setup. The total pressure and total temperature at the cascade inlet and the inlet of coolant feed pipes, as well as the static pressure at the cascade outlet, are also set the same as the experimental study ($P_{0,I} = 180$ kPa, $T_{0,I} = 300$ K, $P_{0,c} = 198$ kPa, $T_{0,c} = 270$ K, $P_{s,c} = 101$ kPa). Because the main focus of the simulation is on tip heat transfer, the boundary condition on the hub is set to be symmetric to reduce the computational cost. The effect of hub end-wall secondary flow on tip leakage flow is considered negligible. No-slip boundary conditions are imposed on all the solid walls.

Isothermal boundary conditions with two different temperatures (250 K and 260 K) are set on all the walls. The wall heat flux from these two cases is subtracted to calculate heat transfer coefficient according to Eq. (1). The assumption here is that heat transfer coefficient only depends on aerodynamics and is independent of the thermal boundary conditions, which is reasonable when the temperature change is small. To determine the cooling effectiveness, another case with adiabatic wall boundary conditions is also calculated.

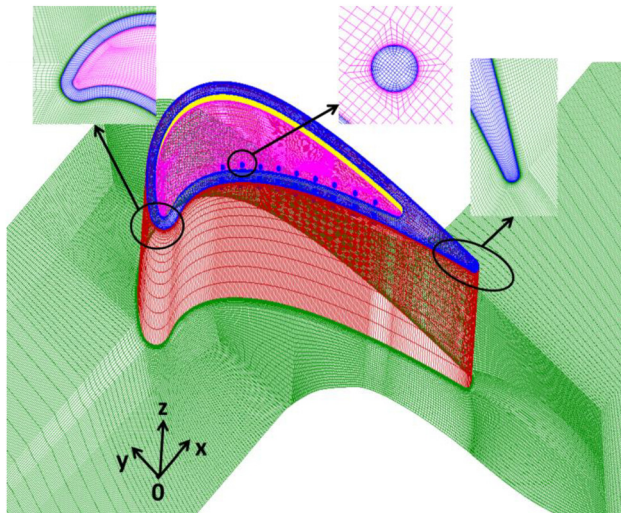


Fig. 7 Computational domain and mesh employed in the present study

Structured mesh with a grid size of 5×10^6 was generated by using Pointwise software. The maximum included angle is controlled within 140 deg. Smooth transitioning is guaranteed at the interface between different mesh blocks. The five-hole case uses the same mesh as the nine-hole case, with additional holes being blocked during numerical computation.

Detailed mesh sensitivity study has been carried out for both Spalart–Allmaras model (SA) and $k-\omega$ SST model (SST). The averaged results are listed in Table 4. For all the cases, average y^+ value on tip surfaces is around one to resolve the near-wall boundary layer. The predicted average value of HTC and adiabatic temperature have relatively large change when the number of grid points across the tip gap is increased from 18 to 30, but their change is only marginal when the tip gap points are further increased to 42.

Figure 8 shows spatially resolved results of the relative difference in HTC between different grid sizes. Generally, the local HTC difference between 5 and 7×10^6 cells is less than one percent for the majority of the tip surface (except some area near the cooling holes). Figure 9 presents the nondimensional radially averaged OTL mass flux over the suction side rim. Grids with 5 – 7×10^6 sizes show same local distribution of leakage flow

Table 4 Mesh and turbulence model dependence studies

Grid size		3×10^6	5×10^6	7×10^6
Grid points within tip gap		18	30	42
Average y^+ on tip surfaces	SA	0.826	0.824	0.823
	SST	0.867	0.883	0.886
Average HTC(W/(m ² -K))	EXP		1199.1	
	SA	1120.5	1102.7	1097.6
	SST	1200.8	1273.8	1301.1
Average $T_{ad}/T_{0,i}$	EXP		0.9800	
	SA	0.9889	0.9887	0.9887
	SST	0.9912	0.9901	0.9903

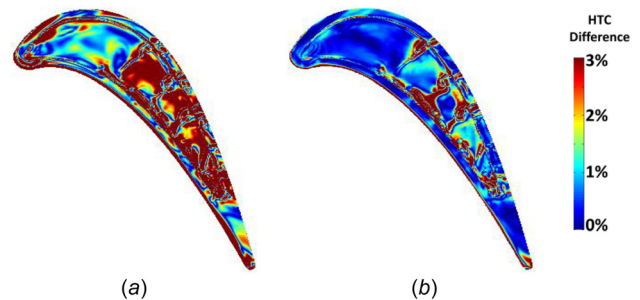


Fig. 8 Contours of the relative difference in HTC between the results from two meshes for the cooled case (PS5): (a) 3 and 5×10^6 and (b) 5 and 7×10^6

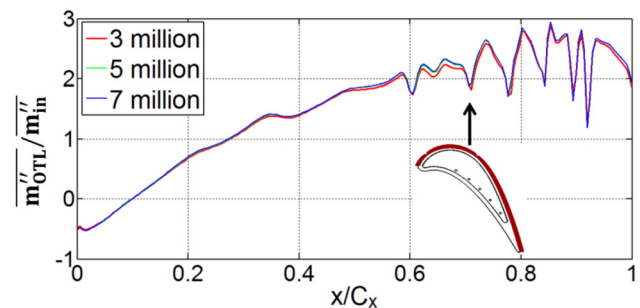


Fig. 9 Nondimensional radially averaged OTL mass flux distribution on the suction side edge of the squealer tip for the cooled case (PS5)

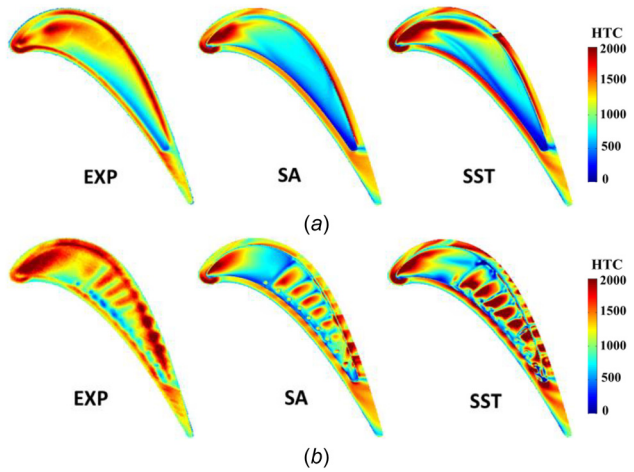


Fig. 10 Contours of HTC on the blade tip surfaces obtained from experiments (EXP) and CFD using SA and $k-\omega$ SST models: (a) uncooled and (b) cooled

along the blade. Therefore, the 5×10^6 mesh is considered adequate for the computations using either SA or SST turbulence model discussed later.

4 Results and Discussion

4.1 Turbulence Model Validation. Figure 10 shows the HTC distributions on the blade tip surfaces obtained from experiments (EXP) and CFD using Spalart–Allmaras model (SA) and $k-\omega$ SST model (SST). For the uncooled case, HTC contour obtained from experiments is well predicted by the two models qualitatively for most of the tip surface. The $k-\omega$ SST model performs better than the SA model in predicting the high HTCs over the cavity floor near the leading edge region. For the cooled case with nine holes near the PS rim, both turbulence models show good qualitative agreement with the experimental HTC distribution. However, the local HTC values near the cooling injection region are over-predicted by the $k-\omega$ SST model by 50% or even bigger. In comparison, the SA model shows a better overall performance in matching the experimental data.

Figure 11 illustrates the circumferentially averaged HTC value along the axial chord. For both the uncooled and the cooled cases, the trend from both experiment and CFD data is consistent. SST model is better than SA model in the prediction of overall quantity. But the local over-prediction by $k-\omega$ SST model in the region of cooling injection is averaged out. The quantitative discrepancy between experiment and CFD is within 30%. This may be caused by the limitation of the RANS models.

SA model has consistently demonstrated its satisfactory performance in predicting tip heat transfer in the recent tip heat transfer studies (Virdi et al. [33], Zhang et al. [24,25], and O’Dowd et al. [29,34]). Results by SA model are further discussed in Secs. 4.1–4.4 and in the Part II paper (Ma et al. [38]).

4.2 Heat Transfer Coefficient. Figure 12 shows the tip HTC distributions for cases with five and nine cooling holes placed near the pressure side rim. Experimental and CFD results show good agreement in the local qualitative pattern. As evident for all the cases shown in Fig. 12, cooling injection introduces some distinctive high HTC stripes on the cavity floor as well as the top of suction side rim. The abrupt HTC variations generally occur between the cooling holes. For both nine-hole and five-hole cases, the peak values and sizes of the HTC stripes on the cavity floor gradually decrease toward the trailing edge, while an opposite trend can be observed over the suction side rim. These heat transfer phenomena have been consistently captured by both

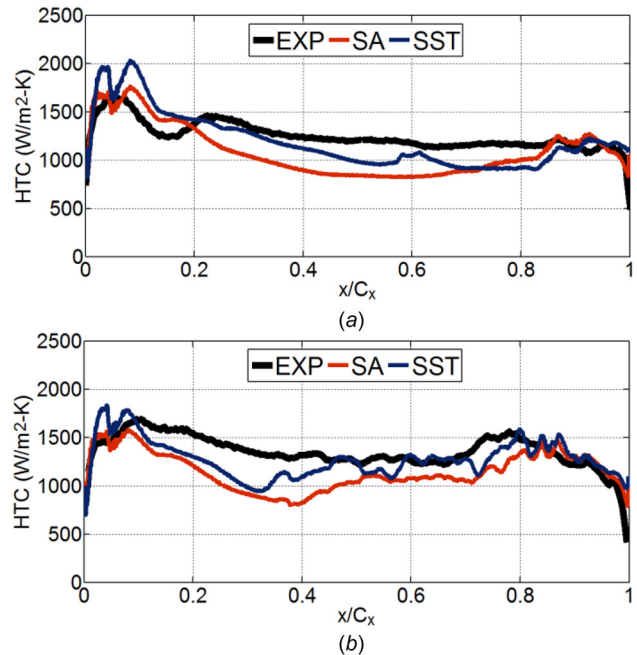


Fig. 11 Circumferentially averaged HTC value: (a) uncooled and (b) cooled

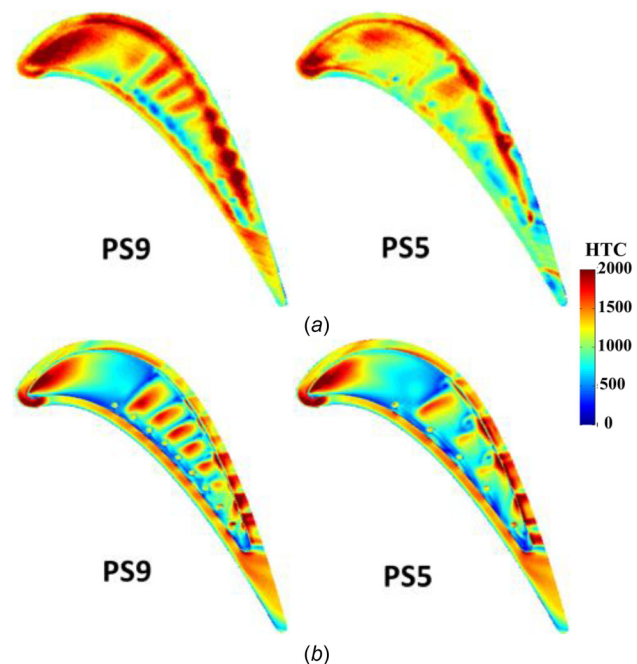


Fig. 12 Contours of HTC for cooling holes near pressure side: (a) EXP and (b) CFD

experiment and CFD, which indicate that some complex interactions between cooling injection and over-tip-leakage flow are to be further exploited. Figure 12 also shows that higher HTC values are associated with the nine-hole case (PS9) in comparison with the five-hole case (PS5), both locally and globally. Potentially this could mean that adding more cooling holes to the squealer tip might not be necessary to guarantee an optimal net heat flux reduction if there is no significant improvement in cooling effectiveness.

Compared with the uncooled squealer shown in Fig. 10(a), the cooled cases in Fig. 12 illustrate an overall remarkable difference

in HTC distributions, which indicates a significant change in tip aerodynamics due to cooling injection.

Figure 13 presents the tip HTC distributions for cooling holes placed along the camberline on the cavity floor. Similar to Fig. 12, distinct HTC stripes can be observed downstream of the cooling injections, especially over the suction side rim. Despite of the qualitative agreement between experiment and CFD, the SA model seems to under-predict the local HTC variations over the cavity floor due to the highly unsteady interaction between the cooling injection and cavity flow.

Figure 14 shows the tip HTC distributions for cooling holes located near the suction side. Different from the other cooling configurations shown in Figs. 12 and 13, the HTC trend in Fig. 14 is quite similar to the uncooled case shown in Fig. 10(a), except the cooling flow signature over the suction side rim.

To sum up, two salient features are consistently observed in both experiment and CFD for several cases. First, distinctive thermal stripes exist on the cavity floor and the SS rim. Second, the strength of these stripes on the cavity floor decreases toward trailing edge, while an opposite trend is observed on the SS rim. These two heat transfer characters signify the strong interaction between the injected coolant and OTL flow.

4.3 Cooling Effectiveness. Contour of cooling effectiveness for the nine-hole case is presented in Fig. 15. In general, both experiment and CFD results show that the cooling effectiveness on most of the tip surfaces is very small, even near the cooling hole region. This is because most of the coolant is lifted off from the surfaces due to the upright injection, as explained in the II paper (Ma et al. [38]). Figure 15 also shows that cooling injection near PS rim can reach the SS rim and give the most coverage area. For the cases with cooling holes near the camberline or SS, some of the coolant is also pushed toward the trailing edge direction by the cavity flow. Similar pattern has been reported by Kwak and Han [19] for squealer tip cooling under subsonic conditions.

4.4 Net Heat Flux Reduction. To assess the combined effect of heat transfer coefficient and cooling effectiveness in engine-

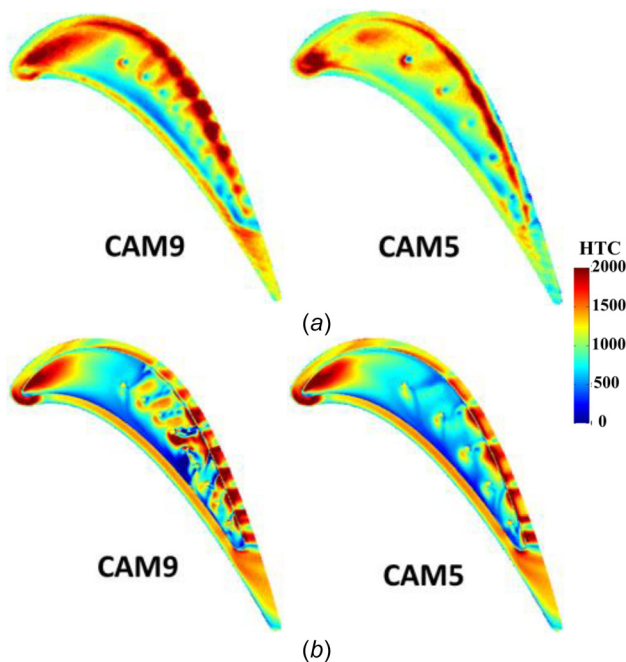


Fig. 13 Contours of HTC for cooling holes along the camberline: (a) EXP and (b) CFD

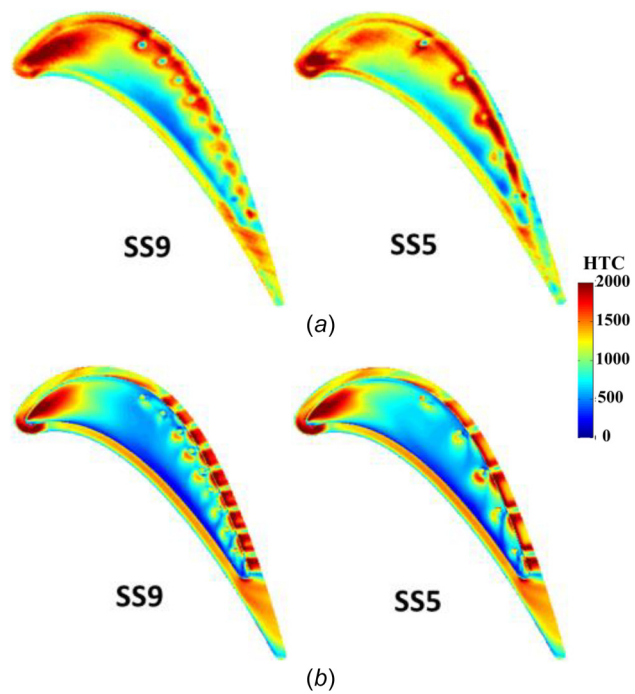


Fig. 14 Contours of HTC for cooling holes near suction side: (a) EXP and (b) CFD

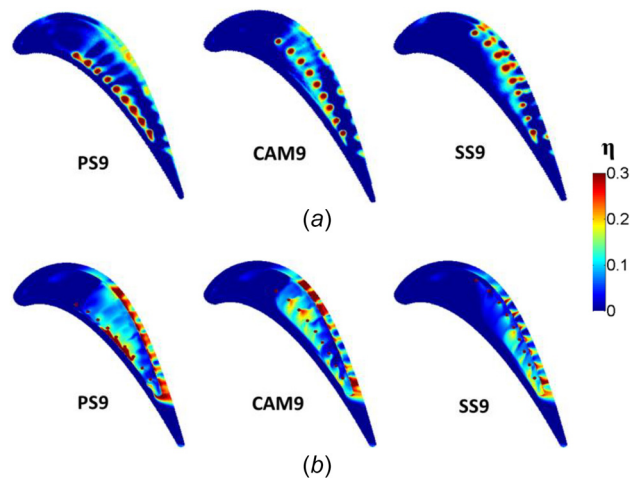


Fig. 15 Contours of cooling effectiveness for the nine-hole case: (a) EXP and (b) CFD

realistic conditions, the net heat flux reduction (NHFR) is defined by Sen et al. [50] and Newton et al. [18] as

$$\text{NHFR} = \frac{q''_{uc} - q''_c}{q''_{uc}} = 1 - \frac{h_c}{h_{uc}} (1 - \eta \Theta_E) \quad (3)$$

The nondimensional engine temperature is defined as

$$\Theta_E = \frac{T_a - T_c}{T_r - T_w} \quad (4)$$

where T_a is the air total temperature (1900 K), T_c is the coolant total temperature (880 K), T_w is the blade metal temperature (1200 K), and T_r is the recovery temperature. In the present study, T_r is derived by multiplying T_a with the recovery factor, which is obtained from the transient thermal measurement for the uncooled case. The assumption here is the recovery factor only depends on aerodynamics and can be scaled up to engine-realistic conditions.

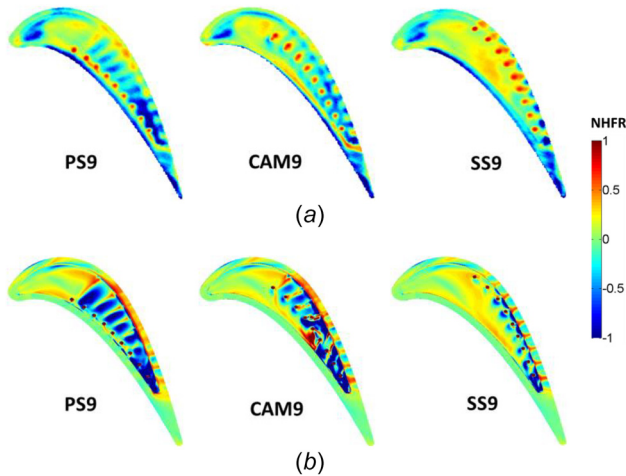


Fig. 16 Contours of net heat flux reduction for the case with nine holes: (a) EXP and (b) CFD

Figure 16 illustrates the contour of net heat flux reduction for the case with nine cooling holes. Experiment and CFD results are in qualitative agreement. They consistently show that net heat flux reduction is positive in regions seemingly unreachable by the coolant, such as the leading edge or upstream of the cooling holes, yet it is negative in regions near the cooling holes where the coolant is supposed to cover. This unexpected result indicates that the strong interaction between the coolant and OTL flow in the tip gap changes the conventional cooling design philosophy obtained on blade surfaces. The interaction mechanism will be elucidated in the Part II paper (Ma et al. [38]).

5 Conclusions

An issue of general interest for HP turbine blade aerothermal designs is to what extent cooling injection from a blade surface would interact with the otherwise uncooled flow pattern. A squealer transonic rotor blade tip is of particular interest, for which there have been no published experimental studies needed for both enhancing the fundamental understanding and providing quality test data with sufficient spatial resolution for CFD validations.

In this two-part paper, a closely combined experimental and CFD investigation into a cooled squealer tip is presented. Here in Part I, experimental and computational setups and results are detailed. Transient thermal measurement data with high resolution are obtained in a high-speed linear cascade (exit Mach number 0.95). To the authors' knowledge, this is the first of the kind of experimental data on the squealer tip cooling under transonic conditions. ANSYS FLUENT was used to simulate all the experimental cases. Detailed CFD sensitivity studies, including mesh dependence studies and turbulence model validations are carried out. The CFD results are qualitatively in good agreement with the experimental data. More importantly, all the relevant phenomena of interest are observed consistently based on both the CFD and the experimental results.

The present results demonstrate strong interactions between over-tip-leakage flow and cooling injection, signified by qualitatively different distributions of surface heat transfer coefficient when cooling injection is introduced. There are distinctive stripe patterns in HTC associated with discrete cooling holes. In addition, there appears to be an opposite trend in chordwise variations of the HTC stripes on the cavity floor compared to that on suction surface rim. Furthermore, a significant change in the net heat flux reduction is identified in the areas seemingly unreachable by the coolant. This may be attributed to the propagated impact on the local flow due to the strong base flow-cooling interactions.

The relevant underlining flow physics and causal vortical flow mechanisms will be examined and discussed in detail in Part II [36].

Acknowledgment

The authors gratefully acknowledge the financial support of Chinese National Science Foundation (51376127), the Innovation Program of Shanghai Municipal Education Commission, and the Aeronautical Scientific Funding.

Nomenclature

CAM	=	camber line
C_x	=	axial chord (m)
d	=	diameter of cooling holes (m)
HP	=	high pressure
HTC, h	=	heat transfer coefficient ($W/(m^2 \cdot K)$)
IR	=	infrared
M	=	Mach number
NHFR	=	net heat flux reduction
OTL	=	over-tip-leakage
P	=	pressure (Pa)
PS	=	pressure side
q''	=	heat flux (W/m^2)
R^2	=	coefficient of determination
SS	=	suction side
T	=	temperature (K)
U	=	uncertainty

Subscripts

ad	=	adiabatic
c	=	coolant, cooled
e	=	exit of linear cascade
i	=	inlet of linear cascade
r	=	recovery
s	=	static
uc	=	uncooled
w	=	wall
0	=	total

Greek Symbols

η	=	cooling effectiveness
Θ_E	=	nondimensional engine temperature

References

- [1] Bunker, R. S., 2001, "A Review of Turbine Blade Tip Heat Transfer," *Ann. N. Y. Acad. Sci.*, **934**(1), pp. 64–79.
- [2] Mayle, R., and Metzger, D., 1982, "Heat Transfer at the Tip of an Unshrouded Turbine Blade," *7th International Conference on Heat Transfer*, Vol. 3, pp. 87–92.
- [3] Bunker, R. S., Bailey, J. C., and Ameri, A. A., 2000, "Heat Transfer and Flow on the First-Stage Blade Tip of a Power Generation Gas Turbine—Part I: Experimental Results," *ASME J. Turbomach.*, **122**(2), pp. 263–271.
- [4] Ameri, A. A., and Bunker, R., 2000, "Heat Transfer and Flow on the First-Stage Blade Tip of a Power Generation Gas Turbine—Part II: Simulation Results," *ASME J. Turbomach.*, **122**(2), pp. 272–277.
- [5] Newton, P., Lock, G., Krishnababu, S., Hodson, H., Dawes, W., Hannis, J., and Whitney, C., 2006, "Heat Transfer and Aerodynamics of Turbine Blade Tips in a Linear Cascade," *ASME J. Turbomach.*, **128**(2), pp. 300–309.
- [6] Krishnababu, S., Newton, P., Dawes, W., Lock, G. D., Hodson, H., Hannis, J., and Whitney, C., 2009, "Aerothermal Investigations of Tip Leakage Flow in Axial Flow Turbines—Part I: Effect of Tip Geometry and Tip Clearance Gap," *ASME J. Turbomach.*, **131**(1), p. 011006.
- [7] Metzger, D., Bunker, R., and Chyu, M., 1989, "Cavity Heat Transfer on a Transverse Grooved Wall in a Narrow Flow Channel," *ASME J. Heat Transfer*, **111**(1), pp. 73–79.
- [8] Chyu, M., Moon, H., and Metzger, D., 1989, "Heat Transfer in the Tip Region of Grooved Turbine Blades," *ASME J. Turbomach.*, **111**(2), pp. 131–138.
- [9] Bunker, R. S., and Bailey, J. C., 2001, "Effect of Squealer Cavity Depth and Oxidation on Turbine Blade Tip Heat Transfer," *ASME Paper No. GT2000-0155*.

- [10] Azad, G. S., Han, J.-C., and Boyle, R. J., 2000, "Heat Transfer and Flow on the Squaler Tip of a Gas Turbine Blade," *ASME J. Turbomach.*, **122**(4), pp. 725–732.
- [11] Azad, G. S., Han, J.-C., Bunker, R. S., and Lee, C. P., 2002, "Effect of Squaler Geometry Arrangement on a Gas Turbine Blade Tip Heat Transfer," *ASME J. Heat Transfer*, **124**(3), pp. 452–459.
- [12] Kwak, J. S., Ahn, J., Han, J. C., Lee, C. P., Bunker, R. S., Boyle, R., and Gaugler, R., 2003, "Heat Transfer Coefficients on the Squaler Tip and Near-Tip Regions of a Gas Turbine Blade With Single or Double Squaler," *ASME J. Turbomach.*, **125**(4), pp. 778–787.
- [13] Zhou, C., and Hodson, H., 2012, "Squaler Geometry Effects on Aerothermal Performance of Tip-Leakage Flow of Cavity Tips," *J. Propul. Power*, **28**(3), pp. 556–567.
- [14] Bunker, R. S., 2006, "Axial Turbine Blade Tips: Function, Design, and Durability," *J. Propul. Power*, **22**(2), pp. 271–285.
- [15] Kwak, J. S., and Han, J. C., 2003, "Heat Transfer Coefficients and Film-Cooling Effectiveness on a Gas Turbine Blade Tip," *ASME J. Heat Transfer*, **125**(3), pp. 494–502.
- [16] Christophel, J. R., and Thole, K. A., 2005, "Cooling the Tip of a Turbine Blade Using Pressure Side Holes—Part I: Adiabatic Effectiveness Measurements," *ASME J. Turbomach.*, **127**(2), pp. 270–277.
- [17] Christophel, J. R., Thole, K. A., and Cunha, F. J., 2005, "Cooling the Tip of a Turbine Blade Using Pressure Side Holes—Part II: Heat Transfer Measurements," *ASME J. Turbomach.*, **127**(2), pp. 278–286.
- [18] Newton, P., Lock, G. D., Krishnababu, S., Hodson, H., Dawes, W., Hannis, J., and Whitney, C., 2009, "Aerothermal Investigations of Tip Leakage Flow in Axial Flow Turbines—Part III: Tip Cooling," *ASME J. Turbomach.*, **131**(1), p. 011008.
- [19] Kwak, J. S., and Han, J. C., 2003, "Heat Transfer Coefficients and Film Cooling Effectiveness on the Squaler Tip of a Gas Turbine Blade," *ASME J. Turbomach.*, **125**(4), pp. 648–657.
- [20] Ahn, J., Mhetras, S., and Han, J.-C., 2005, "Film-Cooling Effectiveness on a Gas Turbine Blade Tip Using Pressure-Sensitive Paint," *ASME J. Heat Transfer*, **127**(5), pp. 521–530.
- [21] Mhetras, S., Narzary, D., Gao, Z., and Han, J.-C., 2008, "Effect of a Cutback Squaler and Cavity Depth on Film-Cooling Effectiveness on a Gas Turbine Blade Tip," *ASME J. Turbomach.*, **130**(2), p. 021002.
- [22] Naik, S., Georgakis, C., Hofer, T., and Lengani, D., 2012, "Heat Transfer and Film Cooling of Blade Tips and Endwalls," *ASME J. Turbomach.*, **134**(4), p. 041004.
- [23] Wheeler, A. P., Atkins, N. R., and He, L., 2011, "Turbine Blade Tip Heat Transfer in Low Speed and High Speed Flows," *ASME J. Turbomach.*, **133**(4), p. 041025.
- [24] Zhang, Q., He, L., Wheeler, A., Ligrani, P., and Cheong, B., 2011, "Overtip Shock Wave Structure and Its Impact on Turbine Blade Tip Heat Transfer," *ASME J. Turbomach.*, **133**(4), p. 041001.
- [25] Zhang, Q., O'Dowd, D., He, L., Oldfield, M., and Ligrani, P., 2011, "Transonic Turbine Blade Tip Aerothermal Performance With Different Tip Gaps—Part I: Tip Heat Transfer," *ASME J. Turbomach.*, **133**(4), p. 041027.
- [26] Zhang, Q., and He, L., 2011, "Overtip Choking and Its Implications on Turbine Blade-Tip Aerodynamic Performance," *J. Propul. Power*, **27**(5), pp. 1008–1014.
- [27] Shyam, V., Ameri, A., and Chen, J.-P., 2012, "Analysis of Unsteady Tip and Endwall Heat Transfer in a Highly Loaded Transonic Turbine Stage," *ASME J. Turbomach.*, **134**(4), p. 041022.
- [28] Zhang, Q., and He, L., 2014, "Impact of Wall Temperature on Turbine Blade Tip Aerothermal Performance," *ASME J. Eng. Gas Turbines Power*, **136**(5), p. 052602.
- [29] O'Dowd, D., Zhang, Q., He, L., Oldfield, M., Ligrani, P., Cheong, B., and Tibbott, I., 2011, "Aerothermal Performance of a Winglet at Engine Representative Mach and Reynolds Numbers," *ASME J. Turbomach.*, **133**(4), p. 041026.
- [30] Anto, K., Xue, S., Ng, W., Zhang, L., and Moon, H., 2013, "Effects of Tip Clearance Gap and Exit Mach Number on Turbine Blade Tip and Near-Tip Heat Transfer," *ASME Paper No. GT2013-94345*.
- [31] Dunn, M., and Haldeman, C., 2000, "Time-Averaged Heat Flux for a Recessed Tip, Lip, and Platform of a Transonic Turbine Blade," *ASME J. Turbomach.*, **122**(4), pp. 692–698.
- [32] Key, N. L., and Arts, T., 2006, "Comparison of Turbine Tip Leakage Flow for Flat Tip and Squaler Tip Geometries at High-Speed Conditions," *ASME J. Turbomach.*, **128**(2), pp. 213–220.
- [33] Virdi, A., Zhang, Q., He, L., Li, H., and Hunsley, R., 2015, "Aerothermal Performance of Shroudless Turbine Blade Tips With Relative Casing Movement Effects," *J. Propul. Power*, **31**(2), pp. 527–536.
- [34] O'Dowd, D., Zhang, Q., He, L., Cheong, B., and Tibbott, I., 2013, "Aerothermal Performance of a Cooled Winglet at Engine Representative Mach and Reynolds Numbers," *ASME J. Turbomach.*, **135**(1), p. 011041.
- [35] Wheeler, A. P., and Saleh, Z., 2013, "Effect of Cooling Injection on Transonic Tip Flows," *J. Propul. Power*, **29**(6), pp. 1374–1381.
- [36] Wang, Z., Zhang, Q., Liu, Y., and He, L., 2015, "Impact of Cooling Injection on the Transonic Over-Tip Leakage Flow and Squaler Aerothermal Design Optimization," *ASME J. Eng. Gas Turbines Power*, **137**(6), p. 062603.
- [37] Zhou, C., 2015, "Thermal Performance of Transonic Cooled Tips in a Turbine Cascade," *J. Propul. Power*, **31**(5), pp. 1–13.
- [38] Ma, H., Zhang, Q., He, L., Wang, Z., and Wang, L., 2016, "Cooling Injection Effect on a Transonic Squaler Tip—Part 2: Analysis of Aerothermal Interaction Physics," *ASME Paper No. GT2016-57587*.
- [39] Zheng, R., Li, M., Wang, Z., and Zhang, Q., 2015, "Control of Blow-Down Wind Tunnel Using Combined Extended and Nonlinear Predictive Filters," *ASME Paper No. GT2015-42908*.
- [40] Xi, J., Zhang, Q., Li, M., and Wang, Z., 2013, "Advanced Flow Control for Supersonic Blowdown Wind Tunnel Using Extended Kalman Filter," *ASME Paper No. GT2013-95281*.
- [41] Ma, H., Wang, Z., Wang, L., Zhang, Q., Yang, Z., and Bao, Y., 2015, "Ramp Heating in High-Speed Transient Thermal Measurement With Reduced Uncertainty," *ASME Paper No. GT2015-43012*.
- [42] Evans, R., Dawes, W., and Zhang, Q., 2013, "Application of Design of Experiment to a Gas Turbine Cascade Test Cell," *ASME Paper No. GT2013-94314*.
- [43] Chen, W., 2013, "Improvements on Conventional Transient Thermal Measurement on Turbine Blade," M.S. thesis, Shanghai Jiao Tong University, Shanghai, China.
- [44] Mee, D., Chiu, H., and Ireland, P., 2002, "Techniques for Detailed Heat Transfer Measurements in Cold Supersonic Blowdown Tunnels Using Thermochromic Liquid Crystals," *Int. J. Heat Mass Transfer*, **45**(16), pp. 3287–3297.
- [45] Kays, W. M., Crawford, M. E., and Weigand, B., 2012, *Convective Heat and Mass Transfer*, McGraw-Hill, New York.
- [46] Oldfield, M. L. G., 2008, "Impulse Response Processing of Transient Heat Transfer Gauge Signals," *ASME J. Turbomach.*, **130**(2), pp. 1–9.
- [47] O'Dowd, D. O., Zhang, Q., He, L., Ligrani, P. M., and Friedrichs, S., 2011, "Comparison of Heat Transfer Measurement Techniques on a Transonic Turbine Blade Tip," *ASME J. Turbomach.*, **133**(2), p. 021028.
- [48] Devore, J., 2011, *Probability and Statistics for Engineering and the Sciences*, Cengage Learning, Boston, MA.
- [49] Coleman, H. W., and Steele, W. G., 2009, *Experimentation, Validation, and Uncertainty Analysis for Engineers*, Wiley, New York.
- [50] Sen, B., Schmidt, D. L., and Bogard, D. G., 1996, "Film Cooling With Compound Angle Holes: Heat Transfer," *ASME J. Turbomach.*, **118**(4), pp. 800–806.